On the prediction of permeability and relative permeability from pore size distributions

Lionel Ecay, David Grégoire, Gilles Pijaudier-Cabot

On the prediction of permeability and relative permeability from pore size distributions

Lionel Ecay[a], David Grégoire[a], Gilles Pijaudier-Cabot [a,*]

[a] *Université de Pau et des Pays de l'Adour, E2S UPPA, CNRS, Total, LFCR, Allée du Parc Montaury, F-64600 Anglet, France*

Abstract

This paper addresses the calculation of the relative permeability of concrete and rocks with a model that is aimed at being implemented in large scale computations for evaluating the tightness of vessels. To this end, it is necessary to rely on some fast procedure and a random hierarchical capillary approach is used. It is based on the extension of an existing model proposed initially to describe the evolution of the intrinsic permeability of mortar undergoing micro-cracking. First, the efficiency of this existing model is tested on several types of concretes and rocks, with permeability spanning over 6 orders of magnitude. Then, the model is adapted to obtain the relative permeability to gas and liquid as a function of the saturation of the porous solid with respect to the liquid phase. The extended model is shown to provide reasonably accurate predictions for several concretes and rocks tested in the literature.

Keywords:

Permeability, Relative Permeability, Pore Size Distribution, Capillary Bundle

1. Introduction

The relationship between the porosity of concrete, mortar, or rocks, and their transfer properties has been a longstanding issue in the literature. There is a wide spectrum of approaches ranging from simple – easy to implement – formulae to complex computational

*Corresponding author
Email address: Gilles.Pijaudier-Cabot@univ-pau.fr (Gilles Pijaudier-Cabot)

schemes. In engineering applications, permeability is often related to the porosity and tortuosity of the material. Garcia-Bengochea *et al.* [1] proposed to describe the fluid flow within the porous material as a parallel bundle composed of capillaries of different diameters. These diameters were distributed according to the void fraction of each pore size obtained from Pore Size Distribution (PSD) measurements which yielded better results than the single diameter approach, see e.g. Kozeny [2]. In more refined approaches, the PSD is entered into an analytical model based on capillary bundles of varying diameters that follow the PSD. For instance, Ait-Mokhtar *et al.* [3] used a simplified bimodal description of the PSD. Amiri and co-workers [4] improved the scheme by using a multimodal description, and Khaddour *et al.* [5, 6] proposed to use the PSD obtained directly from experiments in a random hierarchical assembly of capillary fibers.

Continuum-based up-scaling in which the effective permeability of a heterogeneous material is derived from Darcy's law at the lower scale [7] is the next step in terms of complexity. It provides results where porosity appears explicitly in the evaluation of the effective permeability of the porous material (see e.g. Dormieux *et al.* [8]). *Extensions to non saturated double-porosity media exist in the literature, see e.g. Ref. [9]. These up-scaling techniques are based, however, on Darcy's law at the microscale which turns out not to be valid for gas flow in small pores [5].*

In many instances, porous materials are not saturated by a single fluid in a single phase. In concrete, water condenses in small pores. Hence, water lies in the material's pores in liquid and vapour phases under usual environmental conditions and that drastically affects its transfer properties [10]. The coexistence of more than one phase within the same porous space means that it is possible to transport fluids in different states at the same time and through the same network. Put otherwise, a porous material exhibits several phase-specific intrinsic transport properties at the same time. For a porous material sample subjected to simultaneous gas and liquid permeation, gas (K_g) and liquid (K_l) apparent permeabilities can be measured. With the material's intrinsic permeability K_{in} assessed as well, it is classical

to define the relative gas and liquid permeabilities [11] denoted as k_{rg} and k_{rl} respectively:

$$k_{rg} = \frac{K_g}{K_{\text{in}}} \tag{1}$$

$$k_{rl} = \frac{K_l}{K_{\text{in}}} \tag{2}$$

Several models have been proposed over time in an effort to better predict fluid transport properties for materials in partially saturated states. Key materials that fall within this category are soils, and the first models were developed in the scope of soil studies. A common concept to most of these models is that of an effective saturation level S_r taken as the drainable fraction of porosity:

$$S_r = \frac{S_w - S_{wr}}{1 - S_{wr}} \tag{3}$$

where S_w stands for wetting fluid saturation level (water saturation in most cases) and S_{wr} for wetting fluid residual saturation — saturation at which wetting fluid relative permeability is equal to 0 and at which non-wetting fluid relative permeability is equal to 1. It is worth noting that this residual saturation is not equal to the absolute zero saturation. Indeed, some adsorbed water cannot be extracted and can represent a significant mass proportion while not affecting transport.

Based on the hydraulic radius concept developed by Kozeny [2] and Carman [12], Burdine [13] introduced equations for the wetting and non-wetting fluid relative permeabilities of a porous material. These equations relate the volumetric increments of fluids in the sense of a capillary bundle model to the capillary pressure P_c as defined by the Young-Laplace equation, and to the effective saturation of both wetting and non-wetting fluids. Building on Burdine's work, Corey [14] further simplified the formulae on the basis of experimental evidence relating the inverse of the squared capillary pressure to the wetting fluid saturation level. This greatly simplified the matter, yielding expressions (4) and (5) for wetting and non-wetting fluid relative permeabilities:

$$k_{rw} = S_r^4 \tag{4}$$

$$k_{rnw} = (1 - S_r)^2 \left(1 - S_r^2\right) \tag{5}$$

Later on, Mualem [15] proposed an extension to the Burdine model based on knowledge of the soil-water retention curve and on geometrical assumptions about the porous network. This work was then expanded upon by Van Genuchten [16] and yielded the much-endorsed equation pair for liquid and gas relative permeabilities (6) and (7):

$$k_{rg} = (1 - S_r)^q \cdot \left(1 - S_r^{1/m}\right)^{2m} \tag{6}$$

$$k_{rl} = S_r^q \left(1 - (1 - S_r^{1/m})^m\right)^2 \tag{7}$$

Jason [17] suggested – based on several published results – that an average value of around 0.5 for parameter m is appropriate for cementitious materials, while parameter q values ranging from 3.5 to 5.5 are necessary to account for the strong drop in gas relative permeability at low saturation levels that was not well captured by the original value of 0.5 put forward by Van Genuchten.

Eqs. (6,7) are simple to implement into continuum-scale models that are used for large macro-scale simulations. However, parameters m and q need to be fitted for each pair of porous material and pore fluid. In this sense, the approach is phenomenological, although the original work of Corey provided fixed values of q and m.

The direct approach models fluid transport within the material's actual porous network [18]. The geometry through which transport is computed can be directly obtained via X-ray computed microtomography as demonstrated by Spanne *et al.* [19]. The measured 3D geometry is dependent on the resolution of the apparatus, and current state-of-the-art resolution merely reaches the sub-micrometric scale which is too coarse to accurately represent cementitious materials whose pore diameters can be typically an order of magnitude smaller. In an effort to circumvent these limitations, and partly due to the growing interest in shale gas recovery whose PSD reaches small pores down to a few nanometres in size, a method was developed by Wu *et al.* [20] to generate numerical tridimensional porous structures based on bidimensional thin section images obtained through Scanning Electron Microscopy (SEM). This allows for a tremendous leap in refinement, as SEM enables characterisation down to the scale a few nanometers, as was done by Loucks *et al.* [21] who managed to observe 5 nanometer-wide pores in shales. While this specific application is strongly shale

gas extraction-oriented, these methods could be adapted to cementitious materials.

The real pore structure can be also idealised and viewed as a conjunction of pore bodies connected by narrower pore throats. These are the so-called pore network models. Porosity is modeled as a network of nodes and links, which greatly simplifies the geometry and therefore allows for complex and large simulation boxes. *Accurate pore-network extraction from real porous structures is a research field itself, and one example of of such has been developed by Jiang et al. [22]. A good agreement between Lattice-Boltzmann computed permeability on the original image and pore network model-computed permeability for Berea and Fontainebleau sandstones was obtained.*

Pore network models, e.g. those based on the Lattice-Bolztman approach [23] or on the discrete element method [24], provide permeation properties that derive from the solution of the Stokes problem in the pore network. Because the description lies at the scale where the various fluids can be described separately, multiphase flow can be captured and the relative permeability to wetting and non wetting phases can be approached for a wide variety of fluids [25, 26, 27]. *This is clearly an asset of direct and pore network models compared to phenomenological models that would require to be fitted for each mixture of gas and liquid fluids*.

While powerful and accurate, as they directly solve transport equations, direct and pore network-based models come, however, at a very high computational cost. This prevents their implementation in conjunction with large scale finite element models of structures for which transfer properties are sought. In such applications, models are needed in order to evaluate fluid transport properties at each integration point, and then a boundary value problem is solved at the large scale. Under time-evolving environmental conditions, e.g. in the case of long term ageing of concrete vessels, the saturation distribution evolves and therefore the fluid transfer properties need to be updated, which means that a pore network model, for instance, would need to be run many times. In an effort to devise a fast method that could be used in conjunction with finite element large scale modelling, our aim is to arrive at a model for the prediction of relative permeability that is close to the engineering approach, with as few model parameters as possible.

The present contribution focuses on the transfer of water, in liquid or vapour phases in concrete and rocks. We shall use the random hierarchical bundle model proposed by Khaddour and co-workers [6] as a starting point. The input in this model is the PSD of the porous material, measured according to the mercury intrusion technique (MIP). This model is briefly recalled in the next section. Additional results on intrinsic permeability predictions according to this model over a rather wide variety of porous materials illustrate its efficiency. The extension of the model to the prediction of water and vapour relative permeability as a function of the liquid phase saturation level is discussed in section 3. Comparisons between the model predictions and experimental data available in the literature on the materials considered in section 2 are discussed.

2. Predicting the intrinsic permeability as a function of the pore size distribution

The model that we will be using here is a capillary bundle arranged in a *hierarchical way* – that is from the largest pore diameter to the smallest one – developed by Khaddour *et al.* [6]. This model was initially proposed with two main objectives in mind: the first one was that the model be analytical and has no fitting parameters in order to be fully predictive, and *the second one that the model be able to handle the variation of intrinsic permeability upon gradually increasing damage in the material (although restricted to the pre-peak regime). In order to fulfill this second objective, it was found that the variation of the pore size distribution upon damage due to micro-cracking measured by MIP induced a consistent variation of intrinsic permeability compared to permeation experimental results.* In this paper, we shall restrict the analysis to the prediction of the intrinsic permeability of intact concrete and rocks.

2.1. Review of the Random Hierarchical Bundle Model

The apparent material volume under concern corresponds to a unit weight simply because MIP data is given for unit weight of material and the aim here is to use the rawest data possible, straight out of the apparatus. It is also considered to have a cubic shape defined

by the following set of equations:

$$\begin{cases} V_{\text{app.}} = \frac{V_{\text{void}}}{\Phi} \\ L_s = \sqrt[3]{V_{\text{app.}}} \\ S_s = L_s^2 \end{cases} \tag{8}$$

where $V_{\text{app.}}$ is the unit apparent volume, V_{void} the unit total pore space, Φ the porosity, L_s the unit sample length and S_s the unit sample permeation surface. Assuming cylindrical pore shapes, pore volumes are translated into capillary lengths as follows:

$$L_i = \frac{4V_i}{\pi d_i^2} \tag{9}$$

with L_i, V_i the total length and incremental volume for pore class i of diameter d_i , respectively. Each pore class i is then discretised into equal segments of a random length, which is defined once per class only with computational considerations in mind, as follows:

$$\Delta L_i = n_a \ . \ \min(L_i, L_s) \tag{10}$$

where n_a is a random number equiprobably determined between 0 and 1. This in turn yields a number of pore segments per class n_{pi}:

$$n_{pi} = \left\lfloor \frac{L_i}{\Delta L_i} \right\rfloor \tag{11}$$

The capillary length (same for all) can be defined using tortuosity or not. Here, we will make the same assumption as in Khaddour *et al.* [6] and consider that the assembly length is the sample unit length L_s .

The ground rule for this model is that pore segments can only be assembled from largest to smallest diameter. Segments are assembled by sequentially reading through pore classes starting with the widest one. The model uses a filter probability function in order to decide if a given segment may be placed on active capillaries of ending diameter greater or equal to its diameter or if it will create a new active capillary instead. A capillary is considered active if the combined length of all linked segments has not reached critical length L_s, further

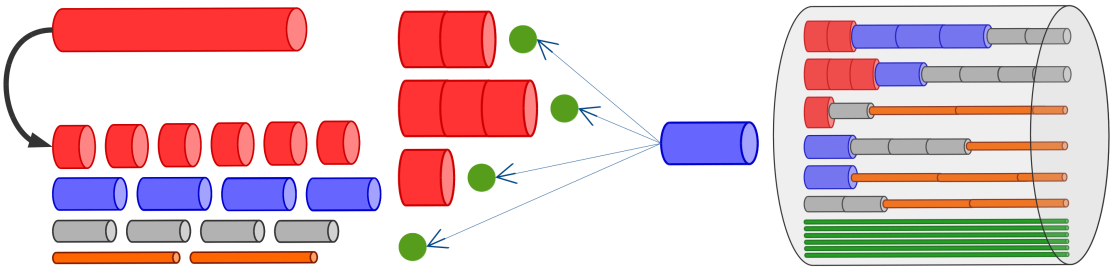

Figure 1: Model process. Left: random discretization; middle: hierarchical assembly; right: completed network (after [6]).

placement of pore segments being possible, and inactive if it has. The main steps of this whole process are shown on figure 1.

The filter probability function $f(j)$ combines a plateau with an exponential decrease as follows:

$$f(j) = \begin{cases} 1, & \text{if } j < B. \\ e^{\frac{B-j}{A}}, & \text{otherwise.} \end{cases} \tag{12}$$

where j stands for the j-th pore segment, B for the threshold under which pore segments have a 100% probability of creating new active sites and A for a parameter driving the exponential slope's steepness, and when pore segments cannot create new capillaries anymore. For every segment another random number n_b between 0 and 1 is computed. If $n_b \leqslant f(j)$ the segment opens a new capillary, while if $n_b > f(j)$ it docks to an existing incomplete one. The graph corresponding to this filter function is shown in figure 2.

As explained in Ref. [6], the threshold B depends on the MIP device. It is calibrated so that, under low pressure where the signal of the device is always very noisy, all segments are assigned to creating active sites. A is a fixed parameter that is set to depend on the accuracy of the assembly scheme: after the completion of each capillary, its permeability is calculated and added to the overall bundle permeability. A threshold is set so that if the permeability increment is below a given value, the assembly process is stopped. The remaining pore segments are then assembled into capillaries of constant diameter. Parameter A is defined so that this threshold is reached before the filter probability function comes too close to zero. Parametric studies [28] have shown that intrinsic permeability predictions are little

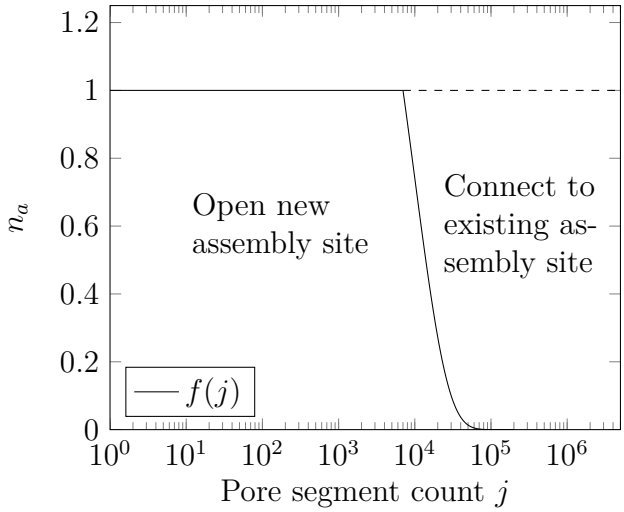

Figure 2: Filter function - $A = 10000$ and $B = 7000$.

sensitive to A provided it is defined as such.

Fluid flow is described at both micro- and macro-scales, the comparison between the two making it possible to retrieve macroscopic physical properties such as permeability while refining the microscopic physics involved. Micro-scale flow is computed, for a compressible gas (such as nitrogen), as a sum of a viscous Poiseuille flow (Eq. 13) and Knudsen molecular diffusion (Eq. 14).

$$Q_{\text{Poiseuille}} = \frac{\pi d^4}{256\mu} \frac{P_1^2 - P_2^2}{LP_2} \tag{13}$$

$$Q_{\text{Knudsen}} = \frac{\pi d^3}{12L}\sqrt{\frac{8RT}{\pi M}}\frac{P_1 - P_2}{P_2} \tag{14}$$

where P_1 and P_2 are the upstream and downstream pressures respectively, for a segment of capillary of length L and diameter d (for details see Khaddour *et al.* [5]). R is the ideal gas constant and T is the temperature.

For every capillary made of m segments of decreasing diameter in the direction of the fluid flow, and using a simple iterative scheme, mass balance conditions provide the fluid flow under known upstream and downstream pressures P_{up} and P_{down}. Then, this fluid flow is summed over the total number of capillaries. Meanwhile, macro-scale flow is described with a classical Darcy equation, and equating it with the sum of the flows in each capillary yields

an explicit analytical equation for the reconstructed porous network's apparent permeability:

$$K_a = \frac{\mu L_s}{S_s} \sum_{i=1}^{n_s} \frac{1}{\sum_{j=1}^{m(i)} \frac{1}{\frac{\pi d_j^4}{L_j} \left(\frac{1}{128\mu} + \frac{1}{12 d_j} \sqrt{\frac{8RT}{\pi M}} \frac{1}{P_{\text{mean},j}} \right)}} \tag{15}$$

where $P_{\text{mean},j}$ is the mean pressure computed in segment j belonging to capillary i. This equation is similar to Klinkenberg's equation in the sense that there is an intrinsic part and another one that depends on the inverse of the mean pressure in each capillary ($1/P_{\text{mean},j}$). Molecular diffusion depends on gas properties and pressure, while what we want to assess is the material's intrinsic permeability, which depends solely on its pore structure. This pressure dependance led Klinkenberg [29] to devise an approach for estimating the intrinsic permeability from a series of flow measurements at different entry pressures: as it increases, the Knudsen proportion in the overall flow decreases. Plotted against the inverse mean pressure, the permeability can be fitted through a linear regression, yielding both the intrinsic permeability as the y-intersect and the Klinkenberg coefficient as the slope, which is a characteristic of the pore network in the material. Typically, narrower pores are more sensitive to diffusion and materials exhibiting finer PSDs will show greater Klinkenberg coefficients.

Before illustrating the main results obtained with this model, it must be remembered that the Random Hierarchical Bundle Model sets the scene for statistical analyses, which implies that repeating the calculations on several capillary bundles is crucial. In the following, each result is the average of several realisations (at least 5 to 10), augmented with a standard deviation. Still, the amount of computing time needed to obtain the average intrinsic permeability remains small enough to envision an implementation in a finite element code where the permeability is to be evaluated at each Gauss point.

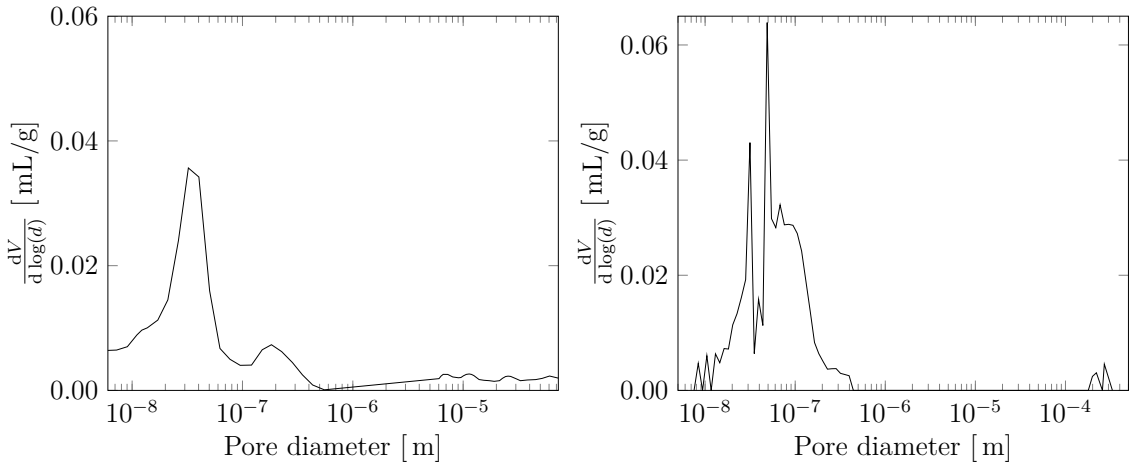

Figure 3: Pore size distribution for CEM I concrete specimens (left, after Chen *et al.*[30]) and for MACENA concrete (right, after Kallel[31]).

2.2. Results

In ref. [6], the model predictions have been initially compared to test data obtained on mortar specimens that have been loaded in uniaxial compression, up to several damage states (viewed as a degradation of the material's Young's modulus). Here we are going to compare the results obtained with this model with data related to other materials that are available in the literature. Among these we have:

- three different concretes reported by Chen *et al.* [30] and Kallel [31] respectively. The first one uses CEM I Portland cement, the second one uses CEM V, highly concentrated in fly ashes and blast-furnace slag. The third one is the concrete used in the MACENA project. The PSD of CEM I and MACENA concretes are shown in Fig. 3;
- Two different rocks: a sandstone tested by Osselin *et al.*[32] which exhibits a PSD that is quite similar to those obtained by Dana and Skoczylas [33] and a Callovo-Oxfordian argilite tested by Andra [34] (Fig. 4).

The parameters in the hierarchical model are $A = 1000$, $B = 8750$ [28]. The intrinsic permeabilities obtained for each material are reported, along with experimental data in table 1. The model stands rather well across a wide range of porous materials spanning six orders

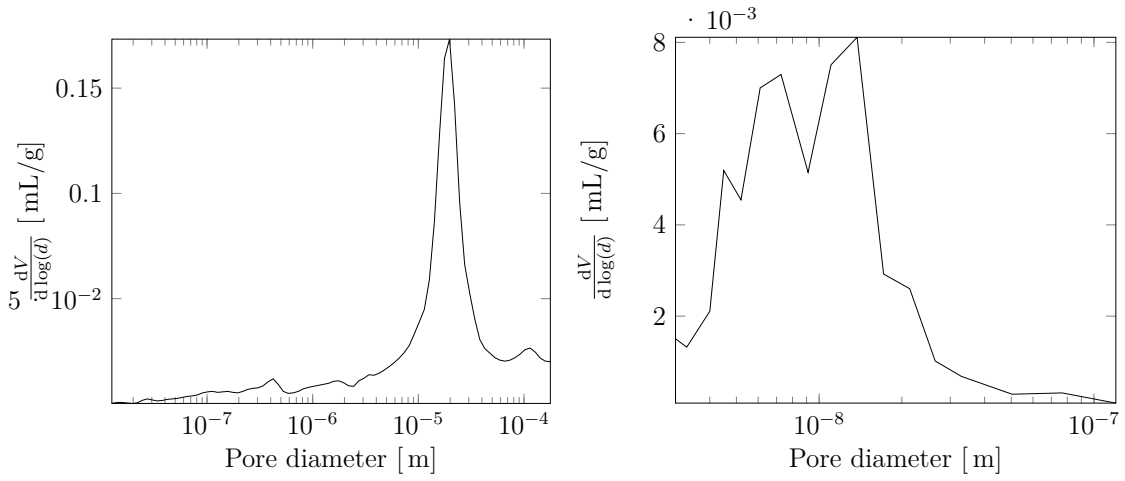

Figure 4: Pore size distribution for sandstone specimens (left, after Osselin *et al.*[32]) and Callovo-Oxfordian argilite (right, after Andra [34]).

Table 1: Experimental and model intrinsic permeabilities.

Specimen	$K_{\text{exp.}}$ [m^2]	K_{model} [m^2]
CEM I	$3.5.10^{-18}$	$[0.7–1.3].10^{-17}$
CEM V	$3.4.10^{-18}$	$[6.4–7.2].10^{-17}$
MACENA concrete	$4.1.10^{-17}$	$[4.1–6.6].10^{-17}$
Sandstone	$1.5.10^{-13}$	$[1.0–1.8].10^{-13}$
Callovo-Oxfordian argilite	$4.2.10^{-19}$	$[3.5–3.7].10^{-19}$

of magnitude in permeability, keeping in mind that there is no fitting parameter. Predictions for the concrete used by Chen *et al.* [30] are less accurate. This discrepancy could come from the fact that the PSD datasets provided by Chen *et al.* were not obtained using the same MIP apparatus. Low-pressure measurement quality depends on the specific apparatus and is related to the probability distribution in Eq. (12). This parameter may vary from one device to the another and could not be checked from the study of Chen *et al.* Also, standard deviations on permeability measurements were not reported and do not appear in this comparison.

It should be noted that these evaluations of intrinsic permeability do not include the effect of the applied stresses (see e.g. the review paper by Hoseini et al. [35] on the effect of stress on concrete permeability). Test data provided by Choinska et al. on concrete [36] show that the effect of an applied uniaxial stress on the apparent permeability is of the order of 5 *to* 10% *at low stress levels that do not induce any material damage. As a matter of fact, the permeability under load is less than the permeability of the unloaded material, which shows that voids - probably the large ones - close upon the application of a compressive load.*

3. Extension to relative permeability

Up until then, the model only considered a porous medium fully saturated with a single fluid, be it either gas or liquid. The reality of porous media is almost always in-between, with the pore space being invaded by a mixture of two phases (liquid water and vapour), one of which is wetting while the other is non-wetting. In cementitious materials, the pore space starts out fully water-saturated when it is cast. Then over time, pore-space water put in contact with an outer atmosphere at a relative humidity lower than 100% gradually evaporates, leading to a non-linear saturation profile inside the material. We are going to expand the hierarchical model in order for it to predict relative permeability for varying saturation levels.

3.1. Modified hierarchical model and redistributive approach

We consider that the medium starts out with its pore space fully saturated with non-wetting fluid, more specifically water vapour in our case. As vapour pressure rises, it eventually reaches a point where it condensates due to confinement within the pore space, as expressed by Kelvin's equation:

$$\ln(RH) = \frac{-2\gamma v_m}{rRT} \tag{16}$$

where RH denotes relative humidity $p_{\text{vapour}}/p_{\text{saturation}}$, $2/r$ stands for meniscus curvature (supposed hemispherical here because perfect wetting and cylindrical pores are assumed), γ stands for surface tension, and v_m stands for the liquid's molar volume.

Because of the way the pore assembly within this model is built, we have a general pore profile consisting of several segments of varying diameters, assembled from wide to narrow. According to Eq. (16), this means that water vapor will first condensate in the last segment of each assembly, the narrower one, and then condensate into segments of growing diameter upon growing relative permeability. From this point out, we can classify three different situations for each capillary:

- if no segment is clogged due to condensation, the capillary is fully vapour-saturated and participates to the vapour flow;
- if at least one but not all segments is clogged due to vapour condensation, the capillary participates neither to gas nor to liquid flow. Also, we do not consider the possibility of the liquid plug being pushed out of the pore due to the pressure gradient. This could be implemented at a later stage, but whether it is relevant or not is open for discussion. Indeed, the idealised view of a pore network assembled from larger to smaller pores is not topologically representative of the actual material, and applying this kind of physics to it might not make sense. Furthermore, one could argue that in the actual material it is more than likely that the smallest pores will be connected at both ends to larger ones and experience smaller pressure differentials than the global one applied to the sample. In this case, little to no plug pushing could occur anyway;
- if liquid is present in all segments, the capillary contributes to the liquid flow.

These three situations are depicted on figure 5. This whole process ties the saturation levels to the PSD of the material and to the volume of each class (diameter) of pore, as all pores of any given size are considered to condensate at the same time. Thus a saturation level can be computed for every pore size.

Note that we are considering here a wetting process, with growing RH, from which a saturation state Sr is derived. A hysteretic behaviour is expected during wetting-drying experiments on $RH - Sr$ graphs but the relationship between the water content saturation Sr and the relative permeability is not expected to exhibit any hysteretic behaviour during

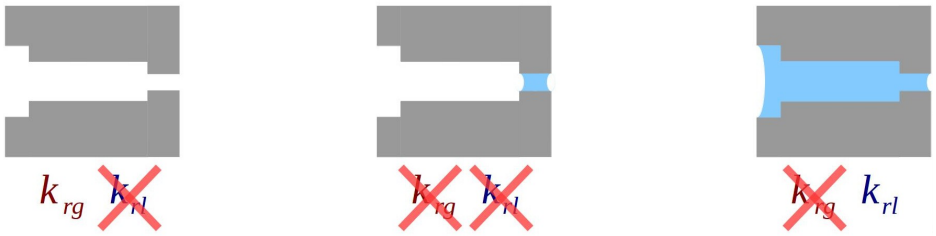

Figure 5: Pore states.

wetting-drying cycles. The relationship between the relative permeability and saturation solely depends on the amount of liquid that may clog the capillaries with respect to the permeation of vapour. As stated by Chen and co-workers [30], the hysteretic response that can be observed on the relative permeability v.s. RH curves shall be recovered due to the hysteretic response of the $RH - Sr$ graphs.

The above rules are not sufficient in order to provide meaningful vapour relative permeability predictions, which could be severely overestimated: it turns out that using such rules, vapour relative permeability is almost constant for saturation states of up to 0.5 in the case of mortar, and steeply drops to zero. Smaller pores – which account for a limited part of the overall permeability when the pore network is saturated with a single fluid – do not have as strong an impact on the decrease of relative permeability to gas at low to moderate water saturation levels as they should. A possible explanation for this discrepancy is that given their significant volume and very small diameters, these pores are expected to come across larger ones with a rather high probability. Such an interconnection between capillaries of different diameters cannot be captured in the hierarchical model which assemble them in parallel only. A combination of parallel and series assembly would be more appropriate, but it goes against the principle of the hierarchical model, and also its simplicity.

Instead, the requirement for the foregoing modified hierarchical model is that small pores should represent a higher proportion of narrow pore throats than they previously did in the initial approach by Khaddour *et al.* [6]. For this, we are going to place tiny segments of these narrower pores at the end of the assembly generated initially. These segments should be small enough so that the intrinsic permeability of the capillary is only slightly affected if at

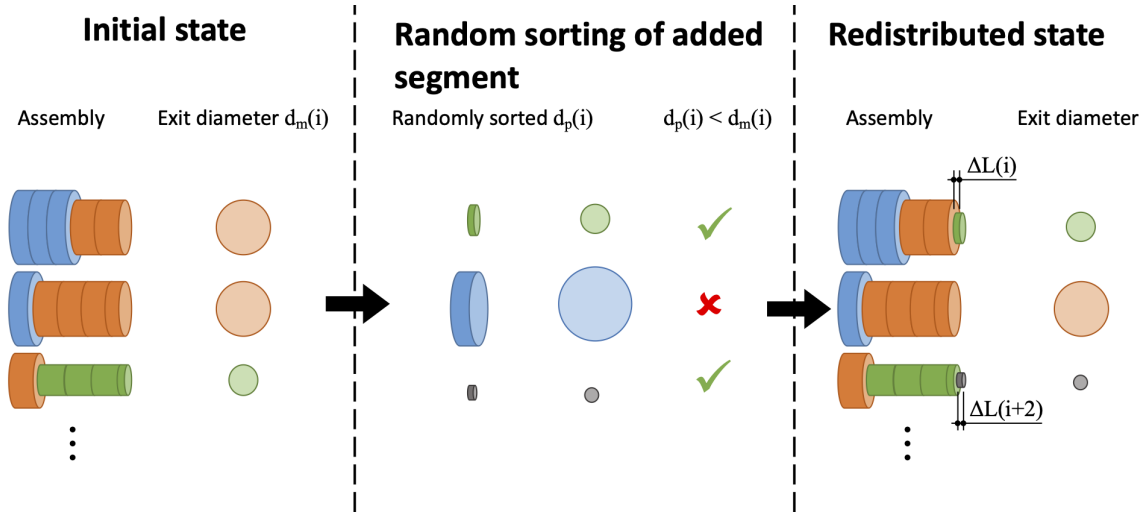

Figure 6: Illustration of the redistributive process: small segments complying to the hierarchical structure of each capillary are added so that the relative permeability to gas is better approached, while keeping at the same time the intrisic permeabilty almost constant.

all. What will henceforth be referred to as *redistributive approach* is the fact of placing short small pore segments downstream of existing capillaries in order to create greater quantities of narrow pore throats. *This redistributive process in illustrated in Fig. (6).*

For this concept to work, length ΔL of the added pore segment j has to be computed by defining a permeability drop for the capillary. This is done by first calculating its permeability without segment j and then postulating a drop in permeability that remains a small fraction of the original, 1% typically. It should be noted here that as the overall permeability is computed as a sum, such an approach merely yields a 1% drop in the global permeability value without any compounding effects. The initial assembly's permeability is given in Eq.(17) and can be compared to its after-redistribution counterpart Eq.(18).

$$K_{\text{in,before}} = \frac{\pi L_s}{128 S_s} \frac{1}{\sum_{i=1}^{m} \left(\frac{L_i}{d_i^4} \right)} \tag{17}$$

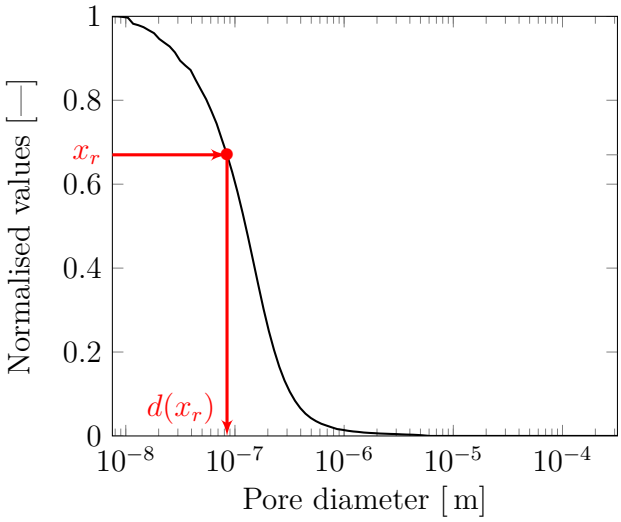

Figure 7: Transfer function – Normalised cumulative pore volume.

$$K_{\text{in,after}} = \frac{\pi(L_s + \Delta L)}{128 S_s} \frac{1}{\sum_{i=1}^{m} \left(\frac{L_i}{d_i^4} \right) + \frac{\Delta L}{d_p^4}} \tag{18}$$

where d_p is the diameter of the added pore segment. Once the permeability drop η is defined, the unknown length ΔL of pore segment j needed to reach the target is obtained as:

$$\Delta L = \frac{\eta \sum_{i=1}^{m} \left(\frac{L_i}{d_i^4} \right)}{\frac{1-\eta}{d_p^4} - \frac{1}{L_s} \sum_{i=1}^{m} \left(\frac{L_i}{d_i^4} \right)} \tag{19}$$

where η is the permeability drop, ΔL the added pore length.

Now that determining the pore length to be adjoined is cleared, a strategy has to be decided about the pore size that will be used. The pore diameter d_p determination will be done randomly and for each capillary. Hence, a transfer function that translates randomly sorted numbers between 0 and 1 into diameters of segments added at the end of each capillary is required.

This transfer function will be arbitrarily chosen, although It should also ideally hold

some form of physical meaning. Our aim is that this transfer function should not introduce additional parameters in the model. Indeed the initial model came to a certain degree of predictivity as far as calculations of intrinsic permeability are concerned, and we would like to try to devise a model for relative permeability without adding any tunable parameter.

We use here the normalised cumulative pore volume curve as the transfer function. An example of such a function is shown on figure 7. The equiprobability of sorting any random number between 0 and 1 means that the added diameter sorting probability density follows the cumulative pore size distribution. There is a higher probability of adding segments of small diameter compared to segments of large diameter at the end of each capillary. Finally, recall that this redistribution should comply with the hierarchical approach, meaning that pore assemblies systematically go from wider to narrower.

The overall redistribution process is organised as follow: once the initial hierarchical bundle (initial configuration) has been created, iterations start covering each capillary from that with the smallest exit diameter to the capillary with the larger exit diameter. For each capillary j, a random number x_r is sorted. As shown in Fig. 7, by reporting x_r on the y-axis, the transfer function provides a corresponding pore diameter $d(x_r) = d_p$ on the x-axis. If d_p is smaller than the exit diameter $d(j)$ of the capillary in the initial state, a segment of length calculated according to Eq. 19 is added at the end this capillary. If d_p is greater or equal to the exit diameter $d(j)$, the capillary is kept unchanged in order to comply with the hierarchical structure of the capillary bundle. Once all capillaries have been considered, the calculation of the relative permeabilities to liquid and vapour can be performed, given a saturation degree, according to the rules illustrated in Fig. (5). This redistribution process yields a slight increase of the volume of the pores for each diameter, which is limited to 2% and therefore considered to be negligible.

3.2. Results

Let us start with the test data on concrete. The results available in the literature deal with the relative permeability to vapour as a function of the water saturation ratio. *Therefore, the validation of the model on concrete specimens will be restricted to the relative*

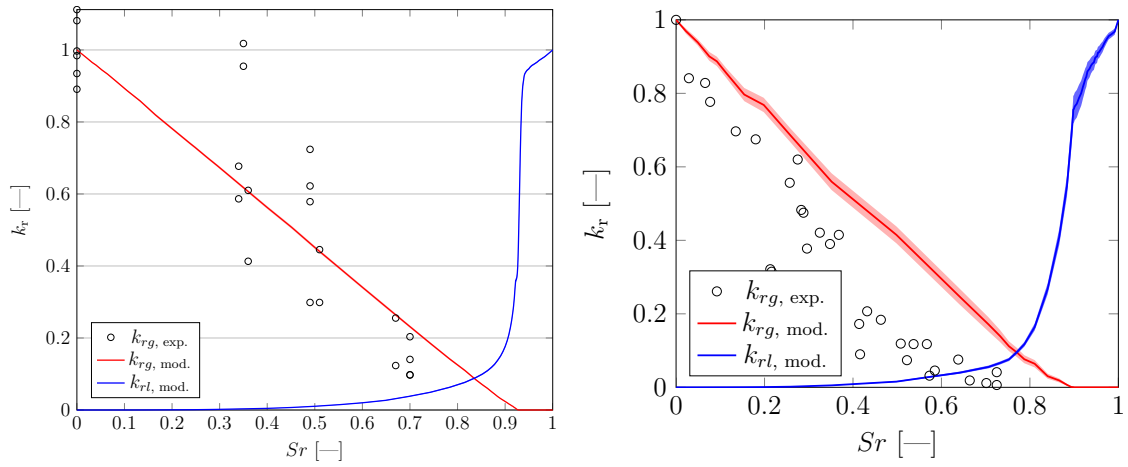

Figure 8: Relative permeability to gas for MACENA concrete[31] (left) and for CEM I concrete used by Chen *et al.*[30] (right).

permeability to vapour only. From the PSD plotted in Fig. (3), relative permeabilities have been computed and compared to experiments. Results are shown in Fig. (8). The figure also shows the relative permeability to liquid water, as an indicative result since experimental data is not available.

While the relative permeability to vapour complies rather well with experimental data and intrinsic permeability is successfully predicted, the wide dispersion of relative permeability measurements is worth noting, for MACENA concrete especially. Model predictions obtained for the CEM I concrete are slightly above experimental data, meaning that smaller pores should have a stronger impact on permeability than they currently do. Nevertheless, considering the fact that the model provides a prediction of relative permeability without any fitting parameter, the error observed in this case should still be acceptable.

For sandstone and Callovo-Oxfordian argilite, the results are shown on Fig. (9). *Experimental results on sandstone are available for the relative permeability to liquid water and gaseous or supercritical carbon dioxyde. A good agreement between the model predictions and experimental data is found, both on the permeability to gas and liquid.* This is probably due to the fact that sandstone has a simple monodisperse strongly peaked PSD compared to concrete. The extended hierarchical model is able to capture both the intrinsic permeability

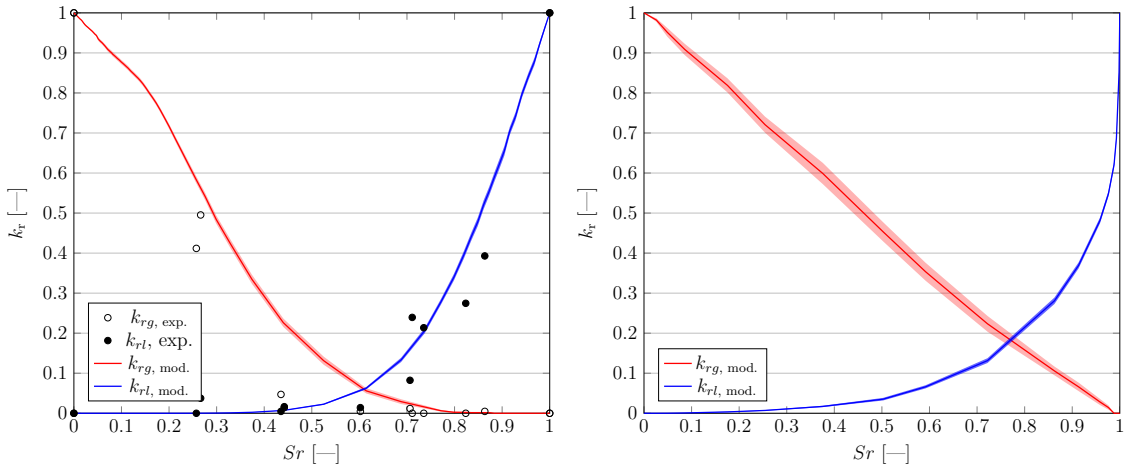

Figure 9: Relative permeability for sandstone[32] (left) and argilite (right).

– although it is four orders of magnitude higher than that of concrete and mortar – and liquid and gas relative permeabilities as well. For low permeability rock such as Callovo-Oxfordian argilite, the relative permeability could not be compared with data from the literature. The reason is that for the PSD used in section 2, the relative permeabilities are not available. Nevertheless, the evolution of the relative permeability to gas with the saturation seems to be qualitatively consistent with data available in the literature on the same type of rock (see e.g. Ref. [37]).

3.3. Evolution of the relative permeability to gas and to liquid upon damage

In the context of ageing concrete structures, it should be informative to determine how the material's relative permeability evolves with damage due to micro-cracking. *Upon micro-cracking, an intrinsic permeability increase is expected, as observed experimentally e.g. in Refs ([6], [36]) and modelled by the hierarchical model where micro-cracks are treated as voids. Here we shall assume, same as in Ref. [6], that micro-cracks act as voids and that their effect on the relative permeability is of the same nature as their effect on intrinsic permeability. Hence, given the PSD for a damaged material, the relative permeability to vapour and liquid water can be computed.* A complete dataset on pore size distribution evolution upon micro-cracking of mortar in uniaxial compression is available in the work of Khaddour *et al.* [6]. The dataset provides the PSD evolution along with intrinsic permeability and

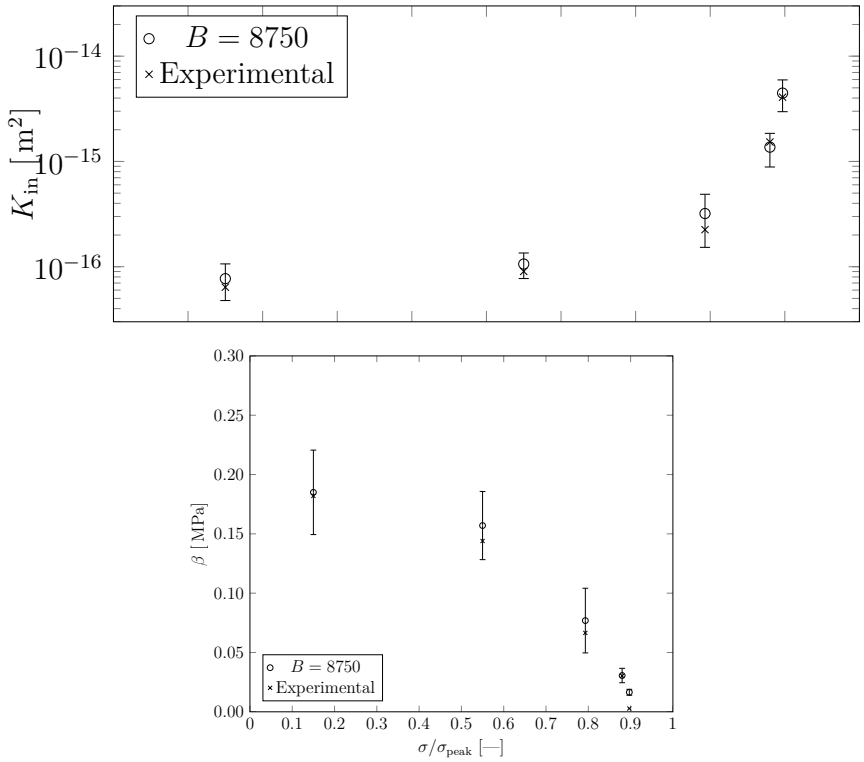

Figure 10: Evolution of the intrinsic permeability (top) and Klinkenberg coefficient (bottom) with damage - comparison with experiments, after Khaddour *et al.* [6].

Klinkenberg coefficient predictions upon damage. Evolutions of the latter two quantities are recalled in Fig. (10).

Fig. (11) shows the evolution of relative permeability to vapour and to liquid water that has been computed from the various PSDs, according to the extended model. In these figures, micro-cracking is described as the degradation of the material's Young's modulus, which goes up to 10% and remains in the pre-peak regime under uniaxial compression.

Several observations can be made: first, the evolution of the relative permeability to vapour seems to be quite insensitive to the state of damage. This had to be expected since the relative permeability to vapour depends on the pores of small diameter and the effect of damage on pores of these diameters is negligible on the PSD. Second, the relative permeability to liquid water is quite influenced by damage. At moderate saturation levels (between 0.5 and 0.8), the relative permeability to liquid water decreases with growing

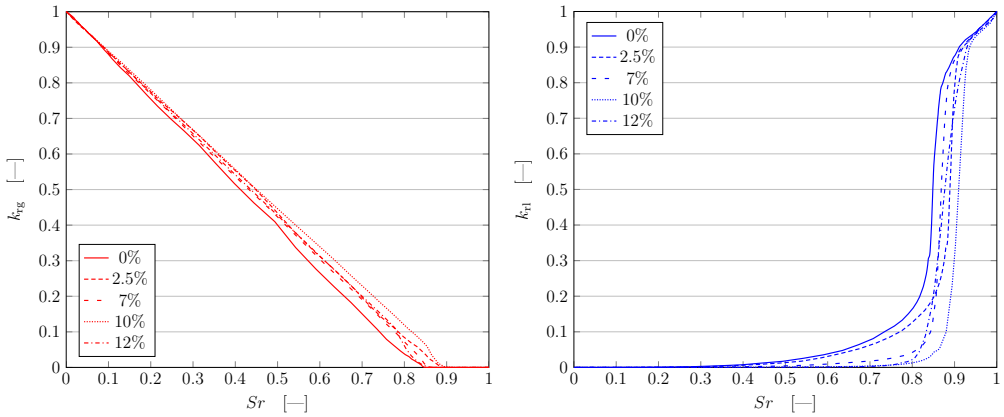

Figure 11: Evolution of the relative permeability to gas (left) and to liquid water (right) of mortar with the liquid water saturation for various states of damage.

damage. The reason for this decrease is that according to Kelvin's law, water will change from the liquid phase to the vapour phase upon an increase in pore diameter. Hence, capillary which were fully saturated with liquid become partially saturated upon an increase of diameter, and they no longer contribute to the liquid relative permeability.

Recall that the intrinsic permeability increases by almost two orders of magnitude when damage grows from 0 to 10%. Hence, the apparent permeability of the damaged material might still increase although the relative permeability decreases. Obviously, these results, which are consistent with the hierarchical approach implemented in the model are still at a preliminary stage. *To our knowledge, experimental data that show the evolution of the relative permeability to vapour and liquid water upon damage are not available in the literature. Therefore, comparisons could not be provided and a proper assessment of the model is pending to this respect.*

4. Conclusions

In this paper, a model aimed at predicting the intrinsic and relative permeability of a porous material has been presented. The model uses the PSD of the material as input, measured according to mercury intrusion porosimetry. It is an extension of the earlier works of Khaddour *et al.* [6] based on a random hierarchical assembly of capillary segments – from

large to small pore diameters. The extension consists in (i) implementing Kelvin's law in order to define the phase (liquid water or vapour) present in the pores, (ii) a set of rules which defines the contribution of each capillary to the transport of liquid and gaseous phases, and (iii) a redistribution of pore segments of small diameters at the end of each capillary in order to better capture their role in the evolution of the relative permeability to gas with liquid-phase saturation. This redistribution is performed according to a function which is similar to the cumulated pore size distribution. The obtained model has no calibration parameter except for one related to the apparatus from which the PSD is obtained.

Comparisons with data from the literature show that the model is capable of providing rather accurate intrinsic permeability predictions for concrete and rocks. Different materials with permeabilities ranging over 6 orders of magnitude have been considered, hereby demonstrating that the model provides consistent results over a wide spectrum of pore size distributions.

Comparisons with data from the literature that provided pore size distributions and vapour relative permeability for concrete and carbon dioxyde – liquid water relative permeabilities for sandstone show that the model provides reasonably accurate predictions of the evolution of the relative permeability with liquid saturation of the pore spaces. The predicted relative permeability to the gaseous phase is above the experimental data, but considering that the model has no tunable parameter once the PSD has been measured, we believe that a reasonable accuracy is achieved. Predicted relative permeabilities are also provided for argilite.

In addition, the model also provides some insight on relative permeability evolution with damage due to micro-cracking. According to the model, relative permeability to vapour is found to be little affected by damage, whereas relative permeability to water decreases with growing damage. These observations need to be confirmed by comparisons with experimental data.

Acknowledgements: this study has been performed with the financial support of ANR through the MACENA project under grant ANR-11-RSNR-0012. The authors would like to gratefully thank Prof. Catherine Davy for kindly providing the pore size distributions of the

concretes tested in the paper by Chen and co-workers [30]. D. Grégoire and G. Pijaudier-Cabot are fellows of Institut Universitaire de France.

References

[1] I. Garcia-Bengochea, A. G. Altschaeffl, C. W. Lovell, Pore distribution and permeability of silty clays, Journal of the Geotechnical Engineering Division 105 (1979) 839–856.

[2] J. Kozeny, Über kapillare Leitung des Wassers im Boden:(Aufstieg, Versickerung und Anwendung auf die Bewässerung), Hölder-Pichler-Tempsky, 1927.

[3] A. Aït-Mokhtar, O. Amiri, P. Dumargue, S. Sammartino, A new model to calculate water permeability of cement-based materials from mip results, Advances in cement research 14 (2002) 43–49.

[4] O. Amiri, A. Aït-Mokhtar, M. Sarhani, Tri-dimensional modelling of cementitious materials permeability from polymodal pore size distribution obtained by mercury intrusion porosimetry tests, Advances in cement research 17 (2005) 39–45.

[5] F. Khaddour, D. Grégoire, G. Pijaudier-Cabot, Capillary bundle model for the computation of the apparent permeability from pore size distributions, European journal of environmental and civil engineering 19 (2015) 168–183.

[6] F. Khaddour, D. Grégoire, G. Pijaudier-Cabot, A hierarchical model for the computation of permeation properties of porous materials and their enhancement due to microcracks, Journal of Engineering Mechanics 144 (2018) 04017160. doi:10.1061/(ASCE)EM.1943-7889.0001392.

[7] H. Darcy, Les fontaines publiques de la ville de Dijon., Exposition et application des principes à suivre et des formules à employer dans les questions de distribution d'eau: ouvrage terminé par un appendice relatif aux fournitures d'eau de plusieurs villes au filtrage des eaux et à la fabrication des tuyaux de fonte, de plomb, de tole et de bitume, Dalmont, 1856.

[8] L. Dormieux, D. Kondo, F. Ulm, Microporomechanics, Wiley Pubs., 2006.

[9] J. Lewandowska, A. Szymkiewicz, M. Burzinski, K.and Vauclin, Modeling of unsaturated water flow in double porosity soils by the homogenization approach, Advances in Wtaer Resources 27 (2004) 283–296.

[10] S. Medjigbodo, M. Choinska, J. regoin, A. Loukili, A. Lhelidj, Experimental study of the air-steam mixture leakage rate through damaged and partially saturated concrete, Materials and Structures 49 (2016) 843–855.

[11] F. Dullien, Porous media: fluid transport and pore structure, Academic press, 2012.

[12] P. C. Carman, Fluid flow through granular beds, Transactions-Institution of Chemical Engineeres 15 (1937) 150–166.

[13] N. Burdine, et al., Relative permeability calculations from pore size distribution data, Journal of Petroleum Technology 5 (1953) 71–78.

[14] A. Corey, The interrelation between gas and oil relative permeabilities, Producers monthly 19 (1954) 38–41.

[15] Y. Mualem, A new model for predicting the hydraulic conductivity of unsaturated porous media, Water resources research 12 (1976) 513–522.

[16] M. T. Van Genuchten, A closed-form equation for predicting the hydraulic conductivity of unsaturated soils, Soil science society of America journal 44 (1980) 892–898.

[17] L. Jason, G. Pijaudier-Cabot, S. Ghavamian, A. Huerta, Hydraulic behaviour of a representative structural volume for containment buildings, Nuclear engineering and design 237 (2007) 1259–1274.

[18] S. Chen, G. D. Doolen, Lattice boltzmann method for fluid flows, Annual review of fluid mechanics 30 (1998) 329–364.

[19] P. Spanne, J. Thovert, C. Jacquin, W. Lindquist, K. Jones, P. Adler, Synchrotron computed microtomography of porous media: topology and transports, Physical Review Letters 73 (1994) 2001.

[20] K. Wu, M. V. Dijke, G. Couples, Z. Jiang, J. Ma, K. Sorbie, J. Crawford, I. Young, X. Zhang, 3d stochastic modelling of heterogeneous porous media–applications to reservoir rocks, Transport in Porous Media 65 (2006) 443–467.

[21] R. G. Loucks, R. M. Reed, S. C. Ruppel, D. M. Jarvie, Morphology, genesis, and distribution of nanometer-scale pores in siliceous mudstones of the mississippian barnett shale, Journal of sedimentary research 79 (2009) 848–861.

[22] Z. Jiang, K. Wu, G. Couples, M. Van Dijke, K. Sorbie, J. Ma, Efficient extraction of networks from three-dimensional porous media, Water Resources Research 43 (2007).

[23] J. White, R. Borja, J. Fredrich, Calculating the effective permeability of sandstone with multiscale lattice boltzmann/finite element simulations, Acta Geotechnica 1 (2006) 195–209.

[24] K. Li, M. Stroeven, P. Stroeven, L. Sluys, Investigation of liquid water and gas permeability of partially saturated cement paste by dem approach, Cement and Concr. Res. 83 (2016) 104–113.

[25] M. Blunt, Flow in porous media - pore network models and multiphase flow, Current Opinions in Colloïd and Interface Science 6 (2001) 197–207.

[26] M. Blunt, M. Jackson, M. Piri, P. Valvatne, Detailed physics, predictive capabilities and macroscopic consequences for pore-network models of multiphase flow, Advances in Water Res. 25 (2002) 1069–1089.

[27] A. Ryazanov, M. Van Dijke, K. Sorbie, Two-phase pore-network modelling: existence of oil layers during water invasion, Transport in Porous Media 80 (2009) 79–99.

[28] L. Ecay, Concrete transfer properties evolution and nuclear vessel tightness assessment during an accident, Ph.D. thesis, Universite de Pau et des Pays de l'Adour, UPPA, Allée du Parc Montaury, Anglet,

France, 2019.

[29] L. Klinkenberg, The permeability of porous media to liquids and gases, in: API Drilling and production practice, American Petroleum Institute, 1941, pp. 200–213.

[30] W. Chen, J. Liu, F. Brue, F. Skoczylas, C. Davy, X. Bourbon, J. Talandier, Water retention and gas relative permeability of two industrial concretes, Cement and Concrete Research 42 (2012) 1001–1013.

[31] H. Kallel, Influence de la température et de l'hygrométrie sur le comportement instantané du béton, Ph.D. thesis, Universite de Pau et des Pays de l'Adour, UPPA, Allée du Parc Montaury, Anglet, France, 2016.

[32] F. Osselin, A. Fabbri, T. Fen-Chong, J.-M. Pereira, A. Lassin, P. Dangla, Experimental investigation of the influence of supercritical state on the relative permeability of vosges sandstone, Comptes Rendus Mécanique 343 (2015) 495–502.

[33] E. Dana, F. Skoczylas, Gas relative permeability and pore structures of sandstones, Int. J. of Rock Mech. and Mining Sc. 36 (1999) 613–625.

[34] Andra, Projet HAVL - Dossier 2005. Referentiel du site de Meuse/Haute-Marne, Technical Report C.RP.ADS.04.0022, Agence nationale de gestion des déchets radioactifs, Châtenay Malabry, France, 2005.

[35] M. Hoseini, V. Bindiganaville, N. Banthia, The effect of mechanical stress on permeability of concrete: A review, Cement and Concr. Composites 31 (2009) 213–220.

[36] M. Choinska, J. Khelidj, G. Chatzigeorgiou, G. Pijaudier-Cabot, Effects and interactions of temperature and stress-level related damage on permeability of concrete, Cement and Concrete Res. 37 (2007) 79–88.

[37] S. M'Jahad, C. Davy, F. Skoczylas, J. Talandier, Characterization of transport and water retention properties of damaged callovo-oxfordian claystone, in: S. Norris, J. Bruno, M. V. Geet, E. Verhoef (Eds.), Radioactive waste confinement: clays in natural and engineered barriers, volume 443 of *Special Publications*, Geological society, London, UK, 2016.